Journal of the European Ceramic Society **18** (1998) 1453–1459

PII: S0955-2219(98)00026-0
0955-2219/98/$—see front matter

Investigations of Alumina/spinel and Alumina/zirconia Interfaces by Spatially Resolved Electron Energy Loss Spectroscopy

K. Suenaga,[a,b]* D. Bouchet,[b] C. Colliex,[b] A. Thorel[a] and D. G. Brandon[c]

[a]Centre des Matériaux Pierre-Marie Fourt, Ecole Nationale Supérieure des Mines de Paris, BP87, 91003 Evry, France
[b]Laboratoire de Physique des Solides associé au CNRS (URA 002), Bâtiment 510, Université Paris-Sud, 91405 Orsay, France
[c]Department of Materials Engineering, Technion—Israel Institute of Technology, Haifa 32000, Israel

(Received 13 August 1997; accepted 2 February 1998)

Abstract

Two types of oxide hetero-interfaces, alumina/spinel and alumina/zirconia, have been investigated by spatially resolved electron energy loss spectroscopy (EELS) with nanometer-scale spatial resolution. Even using the sub-nanometer probe, changes in fine structures in valence and core loss regions across these interfaces are clearly observed and useful information can be successfully derived. We have detected the EELS signal delocalization when interpreting the evolution of the lower energy plasmon of zirconia near the interface and evidenced its energy dependence: the signal delocalization in insulators, such as ceramics, is rather important for the low loss region but practically negligible for the core loss region. Finally some of line-spectra analyses across the interfaces suggest the existence of strongly localized chemical states at the interfaces. These results demonstrate that spatially resolved EELS is a powerful and relevant tool for ceramics characterization at the subnanometer level. © *1998 Elsevier Science Limited. All rights reserved*

1 Introduction

Investigation of local electronic structure with high-spatial resolution is essential for understanding macroscopic phenomena in materials science. As for the ceramic microstructures, the number of spatially resolved electron energy loss spectroscopic (EELS) studies in this field is expanding widely. For example: Bruley has investigated the fine structure changes of Al L_{23}-edge at $\Sigma 11$ boundary in α-alumina.[1] Gu *et al.* have successfully measured the intergranular glassy phase composition in the polycrystalline β-Si_3N_4.[2] The Cr segregation between α-alumina and manganese aluminate spinel ($MgAl_2O_4$) in a metal matrix composite has also been reported by Bruley *et al.*[3] Applications to metal/ceramic interfaces have been performed by Scheu *et al.*[4] and Brydson *et al.*[5] Moreover, an interpretation of the valence energy loss spectra has recently been introduced suggesting an increased ionicity at the $\Sigma 11$ boundary in the α-alumina.[6]

Here we report some results of nano-EELS investigation on oxide hetero-interfaces, alumina/spinel and alumina/zirconia. They are part of a work which originally aimed to reveal the effects of dopants on polycrystalline α-alumina microstructures. We have already reported[7] that doping alumina with Ni leads to the formation of the nickel aluminate spinel ($NiAl_2O_4$) as inter-and intra-granular phases during sintering and that the doping of zirconia into the alumina has also turned out to be an efficient way of controlling the grain growth rate.[8] Therefore, one of the objectives of this paper is to identify the intergranular phases thus corroborating our previous high-resolution works, and to investigate, at the nanometer-level, the changes in local chemistry and chemical state across the interfaces between the alumina matrix and the dispersed grains.

Interpreting data recorded with increased spatial resolution requires a good evaluation of the exact delocalization of the EELS signal. For example,

*To whom correspondence should be addressed;
e-mail: suenaga@lps.u-psud.fr

excitations occuring when electron beams travel parallel and close to hetero-interfaces are now of great interest (e.g. Ref. 9) because interactions of the excitations between the two phases are expected to be non-negligible. It is known that the EELS delocalization is energy-dependent and more important for the valence loss spectrum than for the core loss one. It also depends on the medium through which the electron beam propagates: it is more important in vacuum[10] and less in a metallic material.[11] Our case (especially the alumina/zirconnia interface) provides an interesting system since both media are insulators without any density of states (DOS) at the Fermi-level. Therefore longer Thomas–Fermi's screening lengths are expected than in a conductive specimen. Moreover two well separated plasmon peaks (25·2 eV for alumina and 14·2 eV for zirconia) can be helpful for the quantitative analysis. Here a non-relativistic dielectric theory proposed by Howie *et al.*[12] is introduced to reproduce the low loss evolution near the interface. Then we try to figure out how far local analysis using the spatially resolved EELS technique, can be pushed when applied to characterize insulators, such as ceramics.

2 Experimental

The gel process and co-sintering methods were used for preparation of the doped alumina specimen. The dopants into the investigated samples were pure Ni and yttria-stabilized-zirconia (the tetragonal phase). Detailed preparation procedures for the examined specimens can be found elsewhere.[13] A dedicated STEM VG-HB501 equipped with a Gatan PEELS 666 at the Solid State Physics Laboratory in Orsay was operated at 100 keV for imaging and spectroscopy. The probe sizes were about 0·5 nm for the low loss, Al *L*-edge, Ni *M*-edge and Zr *N*-edge and about 1·2 nm for O *K*-edge acquisitions.[14] A data acquisition and processing mode named 'image-spectrum'[15] allows sequences of EELS spectra to be obtained at pixels regularly spaced on the specimen surface. Here line-scans across the interfaces oriented parallel to the incident beam were recorded with steps of 1·25 or 2·5 nm.

3 Results and Discussions

3.1 Alumina/spinel interface (α-Al_2O_3/$NiAl_2O_4$)

A high angle annular dark field (HAADF) image of the analysed interface is shown in Fig. 1(a). The intergranular spinel ($NiAl_2O_4$) phase of $\sim$0·5 μm in width appears brighter in contrast (for details in quantative calculations of HAADF contrasts, see Ref. 16). The analyzed interface has been selected for several reasons: (1) the region is thin enough for fine structure analysis, (the thickness ratio to the inelastic mean free path is 0·52 and 0·54 for the alumina and spinel grains, respectively); (2) the interface lies almost in perfect edge-on conditions with hardly any tilt; (3) the interface is quite flat and possibly in a preferred orientational condition of (0002)alumina//(111)spinel with parallel oxygen closed packed planes as revealed by diffraction and high resolution works.[7,17] A set of line-scans is acquired along the indicated line across the interface in the figure.

Figure 2 shows variations of the Al L_{23}-, Ni M_{23}-edges and the low loss region across the interface from the alumina grain to the spinel one. (The corresponding spectra are shown from bottom to top in the figure.) The step increment between each spectrum is of 1·25 nm, and the energy dispersion is of 0·21 eV between each energy loss channel. Multiple scattering effects have been removed by Fourier-log deconvolution.[18] In the valence loss spectra, changes in the plasmon peak and other small peaks indicated by arrows are detected when the electron beam is scanned across the interface. The alumina peaks are defined by their positions in the derivative mode at 9·8, 14·7, 20·3 and 32·5 eV. They fit correctly with previously reported ones.[6] The small peaks from the spinel phase are similarly identified at 8·9, 13·9, 18·3, 35·0 and 41·0 eV.

The exact interface position is determined by the spatial evolution of Al L_{23}-edge and Ni M_{23}-edge shown in the right hand side in the figure. (The detailed analysis of these core-loss edges are found in the following paragraphs.) The interface spectrum is modeled by a linear combination of two typical spectra from the alumina and spinel, both recorded far from the interface (typically 10–20 nm away). The difference between the interface spectrum and the best fit spectrum is shown in the uppermost part of the figure. This procedure is not fully valid for the plasmon loss region but represents a first approach to detect any difference between the interface spectra and the bulk spectra. In this procedure the fit is not perfect at the plasmon and the interband transition region (20–40 eV). This difference in the low energy loss region, the origin of which should be further investigated, may imply an interface plasmon mode or changes in ionicity of the interfacial oxygen, as Müllejans and French claimed in their Kramers–Kronig quantitative analyses of the valence loss spectra.[6]

Figure 3 shows the background stripped Al L_{23}-edge and Ni M_{23}-edge fine structures. The energy dispersion for the line-scan is 0·1 eV and the multiple

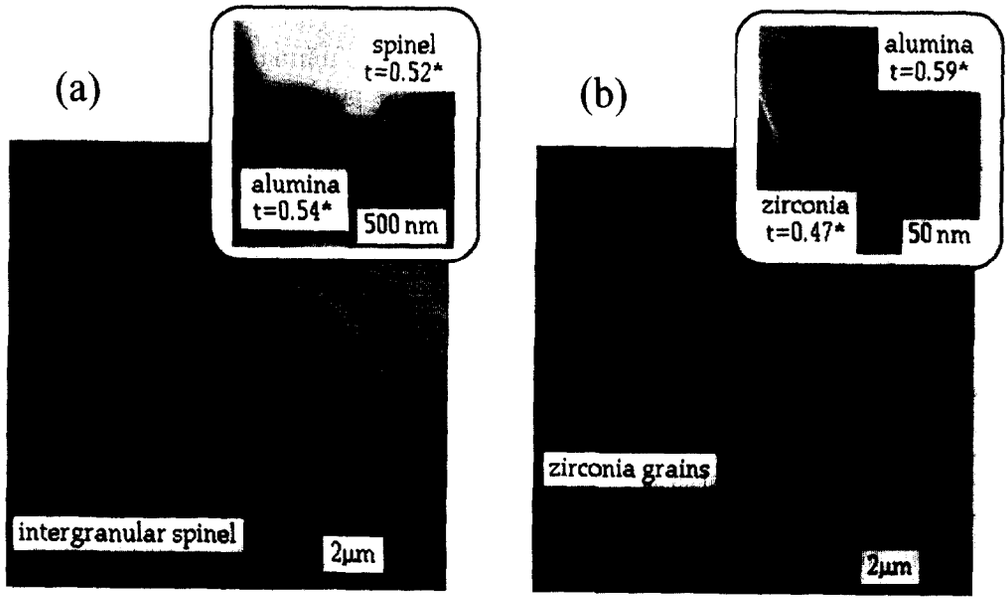

Fig. 1. HAADF images of the explored interfaces (a) alumina/spinel and (b) alumina/zirconia. (a) The intergranular spinel ($NiAl_2O_4$) appears brighter in contrast. The thickness ratio in unites of inelastic mean free path is 0·54 and 0·52 for the analysed alumina and spinel grains. A set of line-spectrum has been acquired along the indicated line. (b) A zirconia grain appears also in brighter contrast rather than an alumina grain. The thickness is 0·47 and 0·59 for the explored grains. Line-scans are recorded along the indicated line.

scattering effects have not been removed. The fine structure of the Al L_{23}-edge from α-alumina shows good similarities with those spectra previously reported[1] and modelled.[19] When acrossing the interface from the α-alumina into the spinel ($NiAl_2O_4$), we can notice several variations associated to the Al L-edge:

1. a hump on the lowest energy peak (A);
2. an increasing intensity in peaks (B) around 84 to 87 eV;
3. a broadening and shifting of the peak (C) towards the lower energy;
4. a lowering in the intensity of the peak (D).

The Al L_{23}-edge structure of the spinel ($NiAl_2O_4$) is similar to that recorded on other spinels by Cadete Santos Aires[20] or by Bruley *et al.*[3] These spinels contain different Al sites coordinated to oxygen.[21] In the case of the nickel aluminate spinel the Al^{3+} cations occupy both octahedral (60%) and tetrahedral sites (40%). Therefore the spinel spectrum could simply be interpreted by superposing those of two different Al sites. A report by Hansen *et al.* contains clear references of the Al L_{23} edges in both octahedral and tetrahedral coordinations to oxygen.[22] In comparison with their work the shoulder of peak (A) is attributed to the tetrahedrally coordinated Al atoms because the octahedrally coordinated Al edge will be similar to that of alumina. Also the lower onset of peak (A) in tetrahedral Al sites is suggestive of a variance in the amount of charge transfer between Al and O atoms.[23] The peak (C) is supposed to reflect Al–O

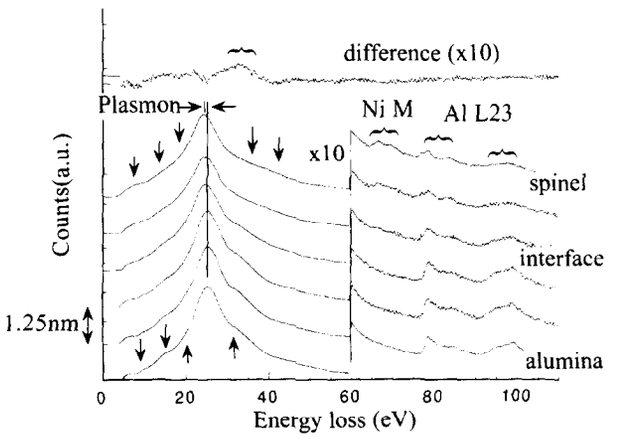

Fig. 2. Variation of the low loss region when the electron beam is scanned across the interface. Each spectrum has been obtained at 1·25 nm increments with the energy dispersion of 0·21 eV. Multiple scattering effects have been removed by the Fourier-log deconvolution. Changes in the plasmon loss, the valence loss and the core loss are detected across the interface. In the uppermost part, the difference between the spectrum from the interface and the best fit obtained from two characteristic spectra is shown.

bond length[5,24]—the position of this peak above the edge onset should vary as $1/R^2$ where R is the bond length. Therefore the broadening in peak (C) represents the different Al–O bond lengths in the spinel structure. The peak (D) is rather higher in energy for the extended structure and must be connected with Al *2s* edge. A workable interpretation of the less intense peak (D) may be a decrease in intensity of the dipole allowed exciation of Al *2s* to Al *3p* states, which may reflect the less ionicity of Al–O bonds with increased *3p* occupancy in spinel than in alumina.

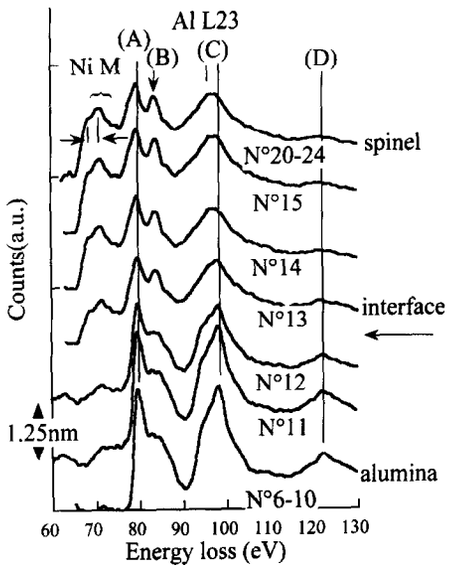

Fig. 3. Background stripped Al *L*-edge and Ni *M*-edge. The channel dispersion for these spectra is 0·1 eV and the increment of each step is 1·25 nm. Variations in the Al *L*-edges can be noticed across the interface from the alumina (bottom) to spinel (top): (A) a small shoulder peak, (B) an increasing intensity of peak, (C) a shift of peak and (D) a lower intensity of peak. The Al *L*-edge of the spinel is interpreted by contributions of two different Al^{3+} cation sites (octahedrally and tetrahedrally coordinated to oxygen atoms), while the *L*-edge of α-alumina consists of only octahedral sited Al^{3+} cations.

Figure 4 shows the oxygen *K*-edge variation across the same interface between alumina and spinel. Here the probe size was 1·2 nm to provide a good signal-to-noise ratio while a probe of 0·5 nm was used for the other edges of lower energies. The increment of the probe position is 2·5 nm. The sharp peak around 536 eV in α-alumina becomes broader and shows a shoulder in the spinel. This shoulder around 532 eV is characteristic to Ni–O bond and attributed to the O *2p* states hybridized with Ni *3d* states.[25] The different structure in the higher energy peaks is due to the different longer range environments in the two materials and involves important information: (i) by measuring the position of peak (C) from the Fermi level the O–O bond length can be deduced; (ii) the peaks (A) and (B) also come from interference effects of backscattered waves on the third or higher coordination shell of the oxygen atoms or cations, therefore multiple scattering calculations, as formerly published by Kurata *et al.*,[24] would be of great help to extract the local higher coordination structure from these fine structures.

Figure 5 gathers the spatial variations of several parameters extracted from the line-scans shown in Figs 2–4. The features are summed up as follows:

1. the Ni M_{23}-edge integrated intensity shows a sharp transition that suggests an abrupt interface.
2. the plasmon peak position varies from 25·2 eV in α-alumina to 24·5 eV in spinel.
3. the position in the energy of the inflection point of peak (A) in the Al L_3-edge exhibits a slight decrease of 1·5 eV through the interface.

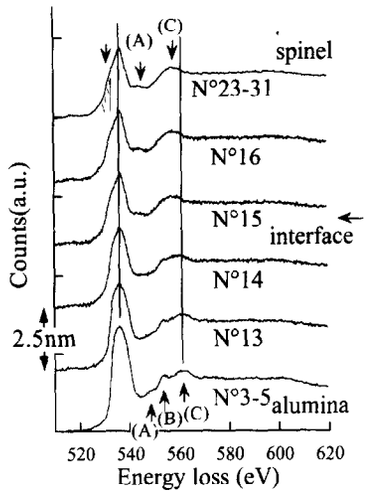

Fig. 4. Oxygen *K*-edge evolution through the interface. The probe size is then 1·2 nm and the step increment is 2·5 nm. The shoulder peak around 532 eV is characteristic to Ni–O bonding and attributed of the O *2p* states hybridized with Ni *3d* states.

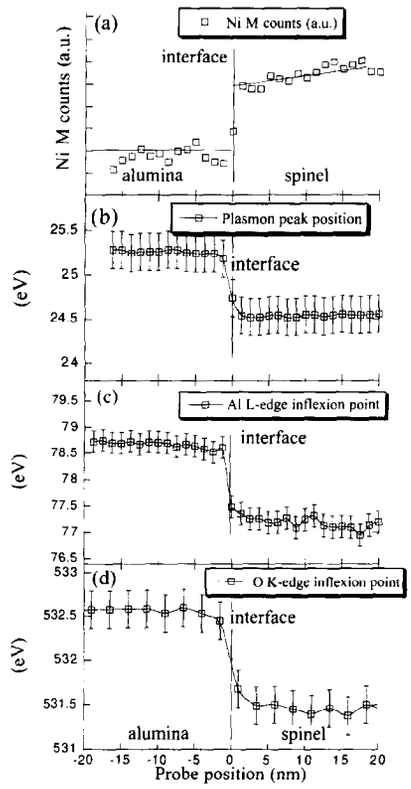

Fig. 5. Spatial variations of several parameters extracted from the line-scans shown in Figs 2–4. (a) Ni *M*-edge intensity shows a sharp changes that suggests an abrupt interface. (b) The plasmon peak position varies from 25·2 eV in α-alumina to 24·5 eV in spinel. (c) The inflection point of peak (A) in the Al L_3 edge shows a decrease of 1·5 eV across the interface. (d) The inflection points of oxygen *K*-edge defined by the first peak positions in the first derivated spectra exhibit a clear change of 1·1 eV through the interface. These values are usable for further phase identifications.

4. the inflection point of oxygen *K*-edge defined by the first peak positions in the derivative spectra shows a clear change of 1·1 eV through the interface. [Note the bigger probe (~1·2 nm) and an increased increment were used for the O *K*-edge acquisition.]

Although it is generally difficult to calibrate the absolute values of core-loss edges, the methods described above are straight forward to measure the exact values of energy shifts. Therefore these quantified evolutions in fine structures provide reliable references when assigning some unknown phases using the finger prints methods.

3.2 Alumina/zirconia interface (α-Al_2O_3/ZrO_2)

An HAADF image of the analyzed interface between zirconia and alumina is shown in Fig. 1(b). The zirconia grain, shown in the left side, appears brighter in Z-contrast. The thickness ratio is 0·47 and 0·59 in terms of the inelastic mean free path in the zirconia and alumina grains. Line-scans are realized along the indicated line through the interface at the centre of the figure.

Variations in the low-loss and the Al $L_{2,3}$-edge, across the interface from zirconia to alumina, are shown in Fig. 6. Both the low loss and the Al $L_{2,3}$-edge are extracted from the same set of the data in a single line-scan. (We can then rule out any problem which arises in aligning line-scans.) In the zirconia, two plasmon (or plasmon associated excitation) are found at (A) 14·2 eV and at (B) 26 eV. According to Camagni *et al.*,[26] the first peak (A) is the bulk plasmon where ε_2 goes minimum and ε_1 is near to zero, while the second peak (B) is still unclear and may be interpreted by an interband transition associated with the plasmon. The small peak at 34 eV and a broader peak at 41 eV are known as Zr N_{23} edge.[27]

An important feature in the evolution of the low loss is a gradual decrease in the intensity of the plasmon (A) *at a few steps (its distance ~4 nm) before the interface*, while, as one can see in the right hand figure, the Al *L*-edge weight changes sharply within two steps (± 1·25 nm) of the interface; this indicates the interface is quite abrupt. The spatial evolution of the intensities of the plasmon (A) and the Al *L*-edge can be seen more clearly in the Fig. 7. The Al *L*-edge intensity has been integrated after the back ground subtraction, while the zirconia plasmon intensity is tentatively defined by the amplitude in the first derivative. The gradual decrease of the plasmon (A) starts about 4 nm away from the interface, while the chemistry changes sharply within two steps (± 1·25 nm).

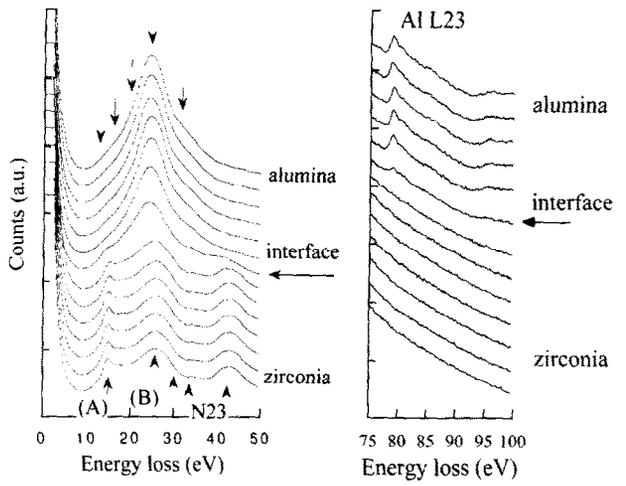

Fig. 6. Variations in low loss and Al *L*-edge across the zirconia to alumina interface shown in Fig. 1(b). Two sets of data are extracted from the same series of a line-scan. In the zirconia part, a double plasmon (or plasmon associated excitation) is found at (A) 14·2 eV and (B) 26 eV. A small peak at 34 eV and a broader peak at 41 eV are known as Zr N_{23} edge. At a few steps before the interface one can see a gradual decrease of the plasmon (A), while the Al *L*-edge's evolution (right hand) suggests an abrupt interface.

This discrepancy is due to the energy dependence of the delocalization of an EELS signal. Using optical data for α-alumina and zirconia[28] we simulate, in Fig. 8, the energy loss excitation probability assuming an electron traveling parallel to and close to the abrupt interface between two materials.* This calculation is based on a non-relativistic dielectric theory proposed by Howie *et al.*[10] which has been shown to model sucessfully experimental EELS spectra for Si/SiO_2 interfaces.[29] The calculated spectra reproduce satisfactorily the spatial dependence of the intense plasmon (A) in the zirconia part near the interface, which has been found experimentally. This interaction distance is dependent on the Thomas–Fermi's screening length of the medium and on the energy loss of the traveling electrons. Muller and Silcox[23] have

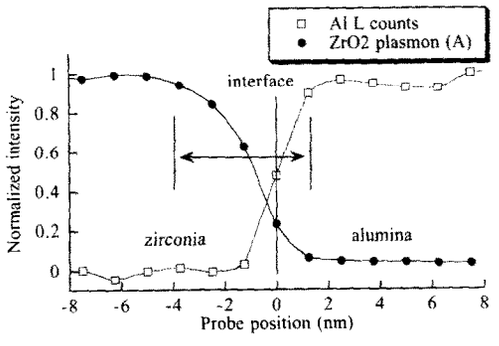

Fig. 7. Spatial variations of the plasmon (A) and the Al *L*-edge intensifies extracted from the same series of the line-scan shown in Fig. 6. The decrease of the plasmon (A) can be detected even at 4 nm apart from the interface, while the chemistry changes sharply within two steps (± 1.25 nm).

*The program named 'inter' is used. This has been elaborated by Z.L. Wang (Georgia Institute of Technology, Atlanta, GA) and modified by P. Moreau.

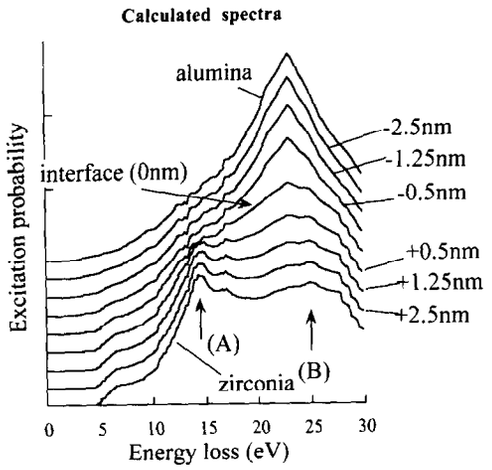

Fig. 8. Simulated electron energy loss spectra based on a non-relativistic dielectric theory, assuming that the electron travels parallel to an abrupt interface with impact distance shown in the right hand side in the figure. The computed spectra can reproduce the behaviour of the less intense plasmon (A) away from the interface.

clearly measured the energy dependence of the EELS signal delocalization into vacuum, where the Thomas–Fermi's screening length is infinite. On the contrary, our recent works of the plasmon analysis at subnanometer-level[23,30] suggest that the delocalization can be negligible even for the low-loss regions in a conductive medium, where quite shorter screening lengths (typically less than 1 angstrom) are expected. The specimens investigated in this paper are insulators without any DOS at the Fermi level, therefore the Thomas–Fermi's screening length is of the order of a few tens nanometers which is between the vacuum and the conductive medium. Then it is quite consistent that the energy dependence of the EELS signal delocalization can be found in this work.

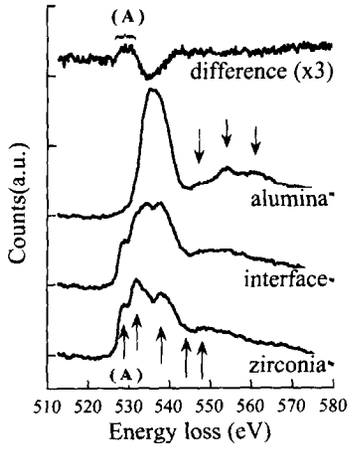

Fig. 9. Changes in oxygen *K*-edge across the alumina/zirconia interface. A quite large core-level shift (about 3·2 eV) can be found through the interface. The O *K*-edge in zirconia exhibits three major peaks and a broader one around 550 eV. The difference between the interfacial spectrum and the best fit of the two typical spectra is shown at the uppermost part of the figure and suggests an increased accomodation of oxygen vacancies at the interface.

Finally the O *K*-edge evolution is shown for another interfacial line-scan in Fig. 9. The O *K*-edge from zirconia has three major peaks as well as a broad peak around 550 eV. The core level shift between alumina and zirconia is large and is estimated to be about 3·2 eV for the peak position in the derivative spectra. Modelling of the interfacial O *K*-edge by the two typical spectra has been performed. The difference between this and the experimental spectrum is shown as the upper curve in Fig. 9. Peak (A) at low energy in the difference spectrum may reveal a local non-stoichiometry of the oxide material. For example, chemical substitution in $SrTi_{1-x}Fe_xO_3$[31] or in a magnetoresistive ceramic $La(Mn_{1-x}Sr_x)O_4$[32] leads to intensity changes in the lowest energy peak of the O *K*-edge. Therefore, in the case of zirconia, the intensity of this peak is supposed to be connected to the amount of oxygen vacancies which are introduced by substituted yttrium atoms into the Zr sites. The increase of this peak intensity found at the interface spectrum therefore suggests that the interface between alumina and zirconia can accommodate more oxygen vacancies than the bulk zirconia does, possibly because of the trivalent feature of aluminium atoms.

4 Conclusion

Investigations of the chemical states at nanometer-level have been carried out across oxide hetero-interfaces using the near-edge fine structure analyses. The changes in valence and core loss regions have been well justified and the results imply further perspective to identify an unknown phase by its electronic structure. Moreover a very localized chemical state for oxygen at the alumina/zirconia interface has been suggested. Finally the calculations based on the non-relativistic theory have modelled the experimental low-loss evolution near the alumina/zirconia interface. This would help practically understanding the EELS signal delocalization in ceramics: One should be careful of the delocalization for the low-loss analysis but the effect can be negligible for core-loss analysis in a typical STEM based nano-EELS configuration. It confirms the great power of the spatially resolved EELS technique when applied to ceramics nanostructure characterization.

Acknowledgements

The authors are most grateful to P. Moreau for his providing a program to calculate the excitation probability based on the non-relativistic dielectric

theory. Thanks to E. Brosh and M. Wei are also acknowledged for their preparation of samples. This work is partially supported by AFIRST program (no. 6052-1-94).

References

1. Bruley, J., Spatially resolved electron energy-loss near-edge structure analysis of a near $\Sigma = 11$ tilt boundary in sapphire. *Microsc. Microanal. Microstruct.*, 1993, **4**, 23–39.
2. Xioqing, P., Gu, H. and Rühle, M., Grain-boundary microstructure and chemistry of a hot isostatically pressed high-purity silicon nitride. *J. Amer. Ceram. Soc.*, 1996, **79**, 2313–2318.
3. Bruley, J., Tseng, M. W. and Williams, D. B., Spectrum-line profile analysis of a mangnesium aluminate spinel/sapphire interface. *Microsc. Microanal. Microstruct.*, 1995, **6**, 1–18.
4. Scheu, C., Dehm, G., Müllejans, H., Brydson, R. and Rühle, M., Electron energy-loss near-edge structure of metal-alumina interfaces. *Microsc. Microanal. Microstruct.*, 1995, **6**, 19–31; Dehm. G, Sheu, C., Möbus, G., Brydson, R. and Rühle, M., Synthesis of analytical and high-resolution transmission electron microscopy to determine the interface structure of Cu/Al_2O_3. *Ultramicrosc.*, 1997, **67**, 207–217.
5. Brydson, R., Müllejans, H., Bruley, J., Trusty, P. A., Sun, X, Yeomans, J. A. and Rühle, M., Spatially resolved electron energy-loss studies of metal–ceramic interfaces in transition metal/alumina cermets. *J. Mircoscopy*, 1995, **177**, 369–386.
6. Müllejans, H. and French, R. H., Interband electronic structure of a near-$\Sigma 11$ grain boundary in α-alumina determined by spatially resolved valence electron energy-loss spectroscopy. *J. Phys. D: Appl. Phys.*, 1996, **29**, 1751–1760.
7. Suenaga, K. M., de Haas, M., Thorel, A., Wei, M., Brosh, E. and Brandon, D. G., Microstructures of polycrystalline alumina stacked with alternate doping. *ler Colloque de Société Francaise des Microscopies*, 1996, pp. 50.
8. Suenaga K., Thorel, A. and Brandon, D. G., Microstructural characterization of Ni/Al_2O_3 diffusion bonds, in preparation.
9. Ugarte, D., Colliex, C. and Trebbia, P., Surface-and interface-plasmon modes on small semiconductiong spheres. *Phys. Rev. B*, 1992, **45**, 4332–4343.
10. Muller, D. A. and Silcox, J., Delocalization in inelastic scattering. *Ultramicrosc*, 1995, **59**, 195–213.
11. Mory, C., Kohl, H., Tence, M. and Colliex, C., Experimental investigation of the ultimate EELS spatial resolution. *Ultramicroscopy*, 1991, **37**, 191–201.
12. Ritchie, R. and Howie, A., Inelastic scattering probabilities in scanning transmission electron microscopy. *Phil. Mag. A*, 1988, **58**, 753–767; Howie, A. and H. Milne, R., Excitations at interfaces and small particles. *Ultramicrosc.*, 1985, **18**, 427–433.
13. Carisey, T., Laugier-Werth, A. and Brandon, D. G., Control of texture in Al_2O_3 by gel-casting. *Journal of the European Ceramic Society*, 1995, **15**, 1–8.
14. Colliex, C., Tencé, M., Lefevre, E., Mory, C., Gu, H., Bouchet, D. and Jeanguillaume, C., Electron energy loss spectrometry mapping. *Mikrochim Acta*, 1994, **114/115**, 71–87.
15. Jeanguillaume, C. and Colliex, C., Spectrum-image: the next step in EELS digital acqusition and processing. *Ultramicr.*, 1989, **28**, 252–257.
16. Suenaga, K., Thorel, A., Houdy, Ph. and Colliex, C., Cross-sectional observation of polymorphic interphases in FeGe multilayers. *Microsc. Microanal. Microstruct.*, 1996, **7**, 143–151.
17. Wasynczuk, J. A. and Rühle, M., in Ceramic Microstrucures '86, pp. 341–346.
18. Egerton, R. F., *Electron Energy Loss Spectroscopy in the Electron Microscope, 2nd Edn. Plenum, New York, 1996.*
19. Tanaka, I. and Adachi, H., Calculation of core-hole excitonic features on Al L_{23}-edge X-ray-absorption spectra of α-Al_2O_3. *Phys. Rev. B*, 1996, **54**, 4604–4608.
20. Cadete Santos Aires, F. J., Cobalt, nickel and copper aluminates characterised by parellel EELS. *Inst. Phys. Conf. Ser.*, 1993, **138**, 55–58.
21. Grimes, R. W, Anderson, A. B. and Heuer, H., Predictions of cation distributions in AB_2O_4 spinels from Normalized Ion Energies. *J. Am. Cem. Soc.*, 1983, **111**, 1–7.
22. Hansen, P. L., Brydson, R., McComb, D. W. and Richardson, I., EELS fingerprint of Al-coordination in silicates. *Microsc. Microanal. Microstruct.*, 1994, **5**, 173–182.
23. Suenaga, K., Colliex, C., Sant, C., Labdi, S. and Houdy, Ph., Electron energy loss spectroscopy with subnanometer resolution on compositionally modulated TiN_x multilayers. *J. Phys. Soc. of Japan*, 1997, **66**, 2097–2102.
24. Kurata, H., Lefevre, E., Colliex, C. and Brydson, R., Electron-energy-loss near-edge structures in the oxygen K-edge spectra of transition-metal oxides. *Phys. Rev. B*, 1993, **47**, 13763–13768.
25. de Groot, F. M. F., Grioni, M., Fuggle, J. C., Ghijsen, J., Sawatzky, G. A. and Petersen, H., Oxygen 1s X-ray-absorption edges of transition-metal oxides. *Phys. Rev. B*, 1989, **40**, 5715–5723.
26. Camagni, P., Samoggia, G., Sangaletti, L., Parmigiani, F. and Zema, N., X-ray-photoemission spectroscopy and optical reflectivity of yttrium-stabilized zirconia. *Phys. Rev. B*, 1994, **50**, 4292–4296.
27. McComb, D. W., Bonding and electronic structure in zirconia pseudopolymorphs investigated by electron energy-loss spectroscopy. *Phys. Rev. B, 1996*, **54**, 7094–7102.
28. Palik, E. D. (ed.), Handbook of Optical Constants of Solids. Academic Press, New York, 1985.
29. Walls, M. G. and Howie, A., Dielectric theory of localised valence energy loss spectroscopy.*Ultramicrosc.*, 1989, **28**, 40–42; Moreau, P., Brun, N., Walsh. C. A., Colliex, C. and Howei, A., Relativistic effects in electron-energy-loss-spectroscopy observations of the Si/SiO_2 interface plasmon peak. *Phys. Rev. B*, 1997, **56**, 6774–6781.
30. Suenaga, K., Colliex C. and Muller D. A., Spatially resolved plasmon analysis at Fe/Ge diffuse interface with steep concentration gradient, in preparation.
31. Steinsvik, S., Bugge, R., Gjonnes, J., Tafto, J. and Norby, T., The defect structure of $SrTi_{1-x}Fe_xO_{3-y}$ ($x = 0$–$0{\cdot}8$) investigated by electrical conductivity measurements and electron energy loss spectroscopy. *J. Phys. Chem Solids*, 1997, **58**, 969–976.
32. Ju, H. L., Sohn, H.-C. and Krishnan, K. M., Evidence for O_{2p} hole-driven conductivity in $La_{1-x}Sr_xMnO_3$ ($0 < x < 0{\cdot}7$) and $La_{0.7}Sr_{0.3}MnO_z$ thin films. *Phys. Rev. Lett.*, 1997, **79**, 3230–3233.